17th World Conference on Earthquake Engineering, 17WCEE
Sendai, Japan - September 13th to 18th 2020

SEISMIC RUBBER BEARING DAMAGE DETECTION USING ELASTIC WAVE PROPAGATION METHOD

M. Ikuta[1], K. Izuno[2] , Y. Kawasaki[3]

[1] *Graduate Student, Ritsumeikan University, rd0069hh@ed.ritsumei.ac.jp*
[2] *Professor, Ritsumeikan University, izuno@se.ritsumei.ac.jp*
[3] *Associate Professor, Ritsumeikan University, yuma-k@fc.ritsumei.ac.jp*

Abstract

Since the 1995 Hyogoken-Nanbu Earthquake, seismic rubber bearings have been used frequently in the construction of highway bridges in Japan. Recently, the deterioration of seismic rubber bearings has been reported after 20 years in service. As the isolation effects of deteriorated bearings during earthquakes are inadequate, early detection of deterioration is necessary to ensure the safety of isolated structures.

The deterioration process of a rubber bearing begins with internal voids in the rubber. However, there is no way to evaluate the presence or absence of internal voids in a seismic rubber bearing without cutting into it. Thus, a nondestructive technique has been required to detect internal voids in seismic rubber bearings.

The authors conducted acoustic emission (AE) measurements to detect internal voids in rubber bearings in the previous studies; however, the propagation paths of elastic waves in rubber layers between steel plates were not clear. Therefore, this study aimed to clarify how elastic waves propagate in rubber using numerical analyses. The wave propagation was simulated using the CIP (Constrained Interpolation Profile) method.

We modeled a seismic rubber bearing as a rectangular parallelepiped, which consists of rubber and steel plates. Our aim was to detect the deterioration utilizing traffic vibration without having to close the road temporarily. Thus, an external force was applied to the top surface of the model assuming the traffic vibration. The external force was expressed as the initial condition of the differential equations.

First, elastic wave propagation was simulated for a healthy bearing without any voids. The waveforms observed at facing observation points were symmetrical, which caused the combined waveform became zero.

Next, we analyzed the case of a deteriorated bearing. The deterioration of rubber bearings usually occurs from a crack in the rubber. Therefore, we assumed a void having a crack-like form as a thin rectangular parallelepiped. The combined waveforms of the observed waves at the facing points showed that the internal void disrupted symmetrical wave propagation.

Thus, the results showed that the internal void can be detected from the combined waves at the observation points facing each other.

Keywords: seismic rubber bearing, damage detection, wave propagation, internal void, CIP method

1. Introduction

Since the 1995 Hyogoken-Nanbu Earthquake, seismic rubber bearings have been used frequently in the construction of highway bridges in Japan. Recently, the deterioration of seismic rubber bearings has been reported after 20 years in service [1]. As the isolation effects of deteriorated bearings during earthquakes are inadequate, early detection of deterioration is necessary to ensure the safety of isolated structures.

The deterioration process of a rubber bearing begins with internal voids in the rubber. However, there is no way to evaluate the presence or absence of internal voids in a seismic rubber bearing without cutting into it. Further, after a massive earthquake, we must be able to distinguish whether we can continue to utilize the bearing, or if we should replace it with a new one. We also have no effective measure other than visual inspection, and we cannot ascertain the degree of internal deterioration due to an earthquake from this inspection. Thus, a nondestructive technique has been required to detect internal voids in seismic rubber bearings.

The authors conducted acoustic emission (AE) measurements to detect internal voids in rubber bearings [2]; however, the propagation paths of elastic waves in rubber layers between steel plates were not clear. Therefore, this study aimed to clarify how elastic waves propagate in rubber using numerical analyses. To verify these results, they were compared to those of the impact elastic wave test. In this study, numerical simulations using a model with an internal void were also conducted, and the effects of a void in a rubber bearing on elastic wave propagation were clarified.

2. Numerical simulation method

The governing equations of three-dimensional (3D) elastodynamics in the stress-velocity formulation assuming linear and infinitesimal deformations are as follows:

$$\rho\partial_t V_x = \partial_x\sigma_{xx} + \partial_y\sigma_{xy} + \partial_z\sigma_{zx} \tag{1}$$
$$\rho\partial_t V_y = \partial_y\sigma_{yy} + \partial_z\sigma_{yz} + \partial_x\sigma_{xy} \tag{2}$$
$$\rho\partial_t V_z = \partial_z\sigma_{zz} + \partial_x\sigma_{zx} + \partial_y\sigma_{yz} \tag{3}$$
$$\partial_t\sigma_{xx} = (\lambda+2\mu)\partial_x V_x + \lambda\partial_y V_y + \lambda\partial_z V_z \tag{4}$$
$$\partial_t\sigma_{yy} = \lambda\partial_x V_x + (\lambda+2\mu)\partial_y V_y + \lambda\partial_z V_z \tag{5}$$
$$\partial_t\sigma_{zz} = \lambda\partial_x V_x + \lambda\partial_y V_y + (\lambda+2\mu)\partial_z V_z \tag{6}$$
$$\partial_t\sigma_{yz} = \mu\partial_z V_y + \mu\partial_y V_z \tag{7}$$
$$\partial_t\sigma_{zx} = \mu\partial_x V_z + \mu\partial_z V_x \tag{8}$$
$$\partial_t\sigma_{xy} = \mu\partial_y V_x + \mu\partial_x V_y \tag{9}$$

where, V is the particle velocity, σ is the stress, λ and μ are Lame's constants, ρ is the density, ∂_t is the partial differential with respect to time t, and $\partial_x, \partial_y, \partial_z$ are the partial differentials with respect to space. The attenuation of the wave with distance is not considered here.

Using the fractional step technique, the 3D problem of Eqs. (1)-(9) can be calculated by one-dimensional (1D) equations. For example, equations in the x-direction are described as Eqs. (10)-(13).

$$\partial_t h_1 + c_L\partial_x h_1 = 0, \quad \partial_t h_2 - c_L\partial_x h_2 = 0 \tag{10}$$
$$\partial_t h_3 + c_T\partial_x h_3 = 0, \quad \partial_t h_4 - c_T\partial_x h_4 = 0 \tag{11}$$
$$\partial_t h_5 + c_T\partial_x h_5 = 0, \quad \partial_t h_6 - c_T\partial_x h_6 = 0 \tag{12}$$
$$\partial_t h_7 = 0, \quad \partial_t h_8 = 0, \quad \partial_t h_9 = 0 \tag{13}$$

where, $h_1 = V_x - \frac{\sigma_{xx}}{c_L\rho}$, $h_2 = V_x + \frac{\sigma_{xx}}{c_L\rho}$, $h_3 = V_y - \frac{\sigma_{xy}}{c_T\rho}$, $h_4 = V_y + \frac{\sigma_{xy}}{c_T\rho}$, $h_5 = V_z - \frac{\sigma_{zx}}{c_T\rho}$, $h_6 = V_z + \frac{\sigma_{zx}}{c_T\rho}$, $h_7 = \sigma_{yy} - \frac{\lambda}{\lambda+2\mu}\sigma_{xx}$, $h_8 = \sigma_{zz} - \frac{\lambda}{\lambda+2\mu}\sigma_{xx}$, $h_9 = \sigma_{yz}$, $c_L = \sqrt{\frac{\lambda+2\mu}{\rho}}$, and $c_T = \sqrt{\frac{\mu}{\rho}}$.

From Eq. (13), h_7, h_8 and h_9 do not vary with time. Eqs. (10)-(12) are 1D advection equations according to the longitudinal wave speed c_L and the transverse wave speed c_T.

This study solves these advection equations using the RCIP (Rational-Constrained Interpolation Profile) method [3]. This method assumes that the spatial derivative of the variables also propagates according to the advection equations. If we denote g_i as the spatial derivative with respect to the x-direction of h_i (i=1, 2, ...6), h_i and g_i can be obtained using the RCIP method. As the space derivative with respect to the y- and z-directions of h_i are not obtained from the advection equations in the x-direction, $\partial_y h_i$ and $\partial_z h_i$ are calculated from g_i using the central difference method [4]. Then, these schemes were applied to the y- and z-directions.

We modeled a seismic rubber bearing as a rectangular parallelepiped, and set this model with sides parallel to the coordinate axes as shown in Fig. 1. The dimensions of this model were 106 mm × 180 mm × 180 mm. As the boundary of this model is orthogonal to the axes, the boundary conditions at free surfaces are satisfied by assuming the appropriate virtual incoming wave from outside of the domain [5]. For example, the boundary conditions for the x-direction are as follows:

$$h_1 = h_2, \quad h_3 = h_4, \quad h_5 = h_6 \tag{14}$$
$$\partial_x h_1 = -\partial_x h_2, \quad \partial_x h_3 = -\partial_x h_4, \quad \partial_x h_5 = -\partial_x h_6 \tag{15}$$
$$\partial_y h_1 = \partial_y h_2, \quad \partial_y h_3 = \partial_y h_4, \quad \partial_y h_5 = \partial_y h_6 \tag{16}$$
$$\partial_z h_1 = \partial_z h_2, \quad \partial_z h_3 = \partial_z h_4, \quad \partial_z h_5 = \partial_z h_6 \tag{17}$$

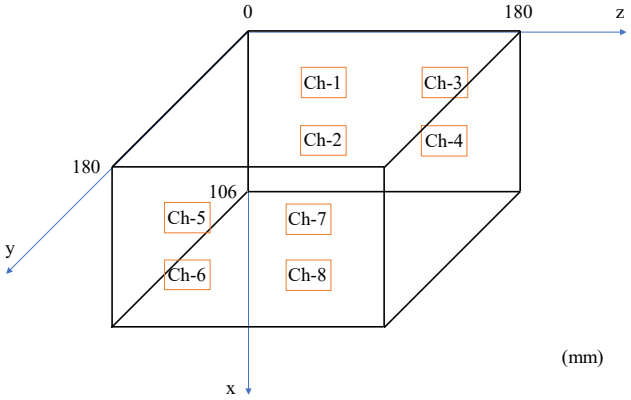

Fig. 1 – Dimensions of specimen

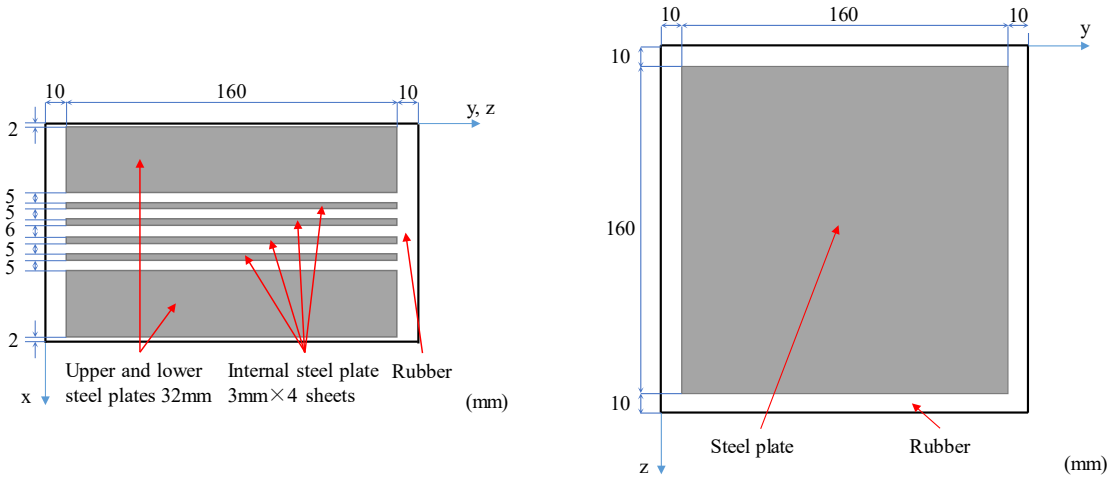

Fig. 2 – Steel plates layout

The seismic bearing consists of rubber and steel plates as shown in Fig. 2. The dimensions of the upper and lower steel plates are 32 mm × 160 mm × 160 mm, and those of the internal plates are 3 mm × 160 mm × 160 mm.

Table 1 shows the locations of the observation points. Eight sensors were located symmetrically.

The reflection of waves due to the internal void was also considered. The deterioration of rubber bearings usually occurs from a crack in the rubber. Therefore, we assumed a void having a crack-like form as a thin rectangular parallelepiped. The propagated waves reflect at the surface of the internal void in the same manner as the free surface of the model.

Our aim was to detect the deterioration utilizing traffic vibration without having to close the road temporarily. Thus, an external force was applied to the top surface of the model assuming the traffic vibration. The external force was expressed as the initial condition of the differential equations. The particle velocity in the x-direction V_x was set to 1 m/s for the entire surface at $x = 0$.

Table 1 – Observation point locations

		Observation point							
		Ch-1	Ch-2	Ch-3	Ch-4	Ch-5	Ch-6	Ch-7	Ch-8
Coordinate	x (mm)	34	72	34	72	34	72	34	72
	y (mm)	0	0	0	0	180	180	180	180
	z (mm)	30	30	150	150	30	30	150	150

In our previous study [6], a specimen of G10 rubber meeting the specifications of the Japanese Industrial Standards; JIS was used to verify the propagation speed of an elastic wave in rubber. This study assumed the same elastic properties as the specimen in the previous study, i.e., the elastic shear modulus $G = 1.0$ MPa, the density $\rho = 1{,}140$ kg/m^3, and Poisson's ratio $\nu = 0.49983$. Then the longitudinal speed c_L and the transverse speed c_T are expressed as Eq. (18) using G, ρ and ν.

$$c_L = \sqrt{\frac{2G}{\rho}\frac{1-\nu}{1-2\nu}} \quad , \qquad c_T = \sqrt{\frac{G}{\rho}} \tag{18}$$

From Eq. (18), the longitudinal speed c_L is 1600 m/s, while the transverse speed c_T is 30 m/s which is less than 1/50 of c_L.

We used 1 mm cubic grids and the time increment $\Delta t = 0.2$ μs in order to satisfy a Courant number of about 0.5, and applied a moving average to get data every 1 μs.

3. Internal void detection

3.1 Healthy bearing

First, elastic wave propagation was simulated for a healthy bearing without any voids. Figure 3 shows the particle velocity-time histories at the observation points. The waves observed at the points with the same x-coordinates are the same, i.e., Ch-1 and Ch-3. Further, the waveforms observed at facing observation points were symmetrical, i.e., Ch-1 and Ch-5. In the next section, we use this symmetrical phenomenon to detect internal voids.

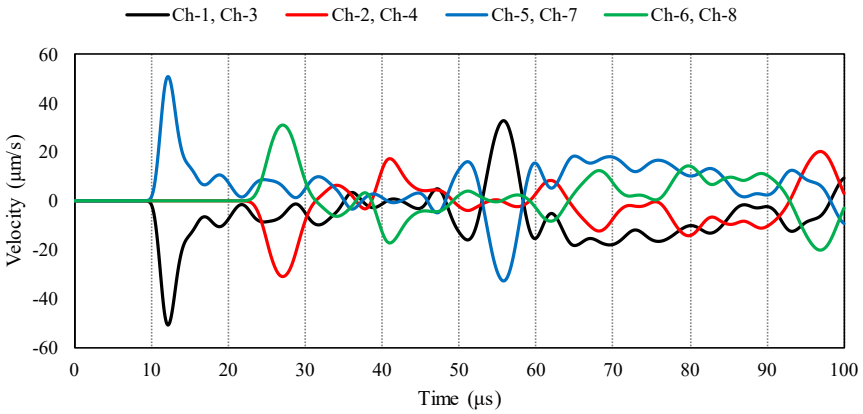

Fig.3 – Particle velocity-time histories

3.2 Bearing with internal void

Next, we analyzed the case with an internal void. A crack was modeled as the internal void. We assumed an internal void measuring 1 mm × 10 mm × 10 mm below the internal steel plate at (x, y, z) = (42.5, 15, 165) as shown in Fig.4.

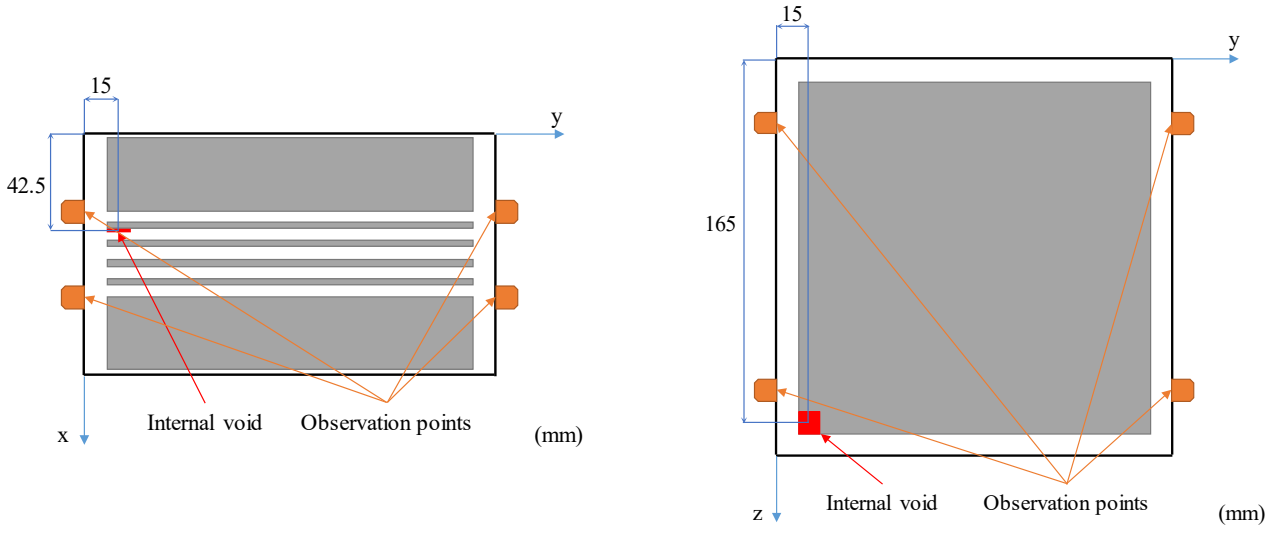

Fig.4 – Internal void position

The observed particle velocity-time histories are shown in Fig. 5. If the waveforms at the facing points were symmetrical, the combined waveform became zero. Figure 6 shows the combined waveforms of the waves at the facing points derived from Fig. 5. These non-zero waves showed that the internal void disrupted symmetrical wave propagation.

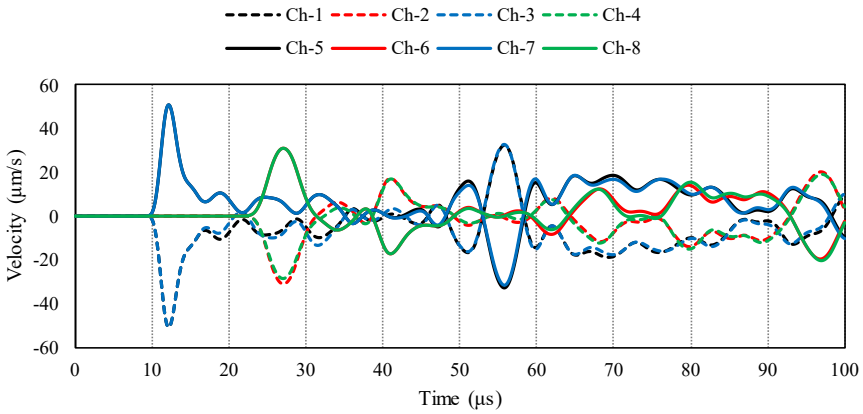

Fig. 5 – Observed propagated waves

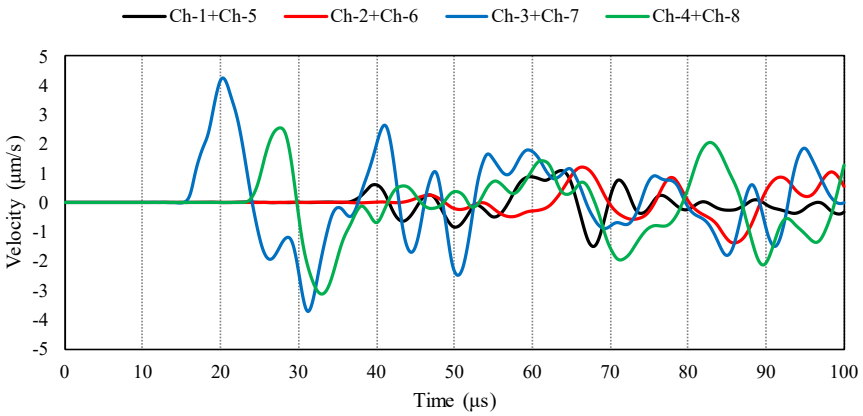

Fig. 6 – Combined waveforms

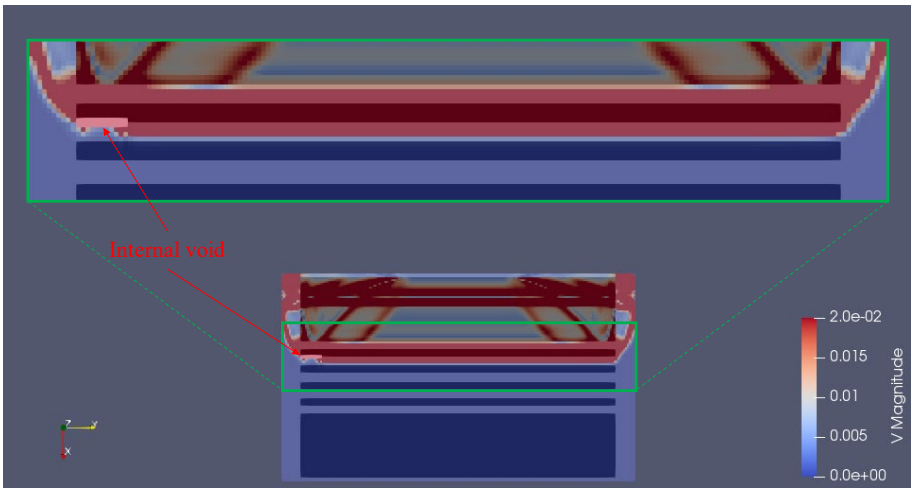

Fig. 7 – Distribution of absolute particle velocity at 10μs

Table 2 – Maximum values of Fig. 6

	Ch-1+Ch-5	Ch-2+Ch-6	Ch-3+Ch-7	Ch-4+Ch-8
Velocity (μm/s)	1.09	1.21	4.25	2.55

Figure 7 shows the distribution of the absolute particle velocity at 10 μs. The reflected waves from the internal void caused interference and disrupted the symmetry of wave propagation.

Table 2 shows the maximum values of Fig. 6. As the assumed internal void was located near Ch-3, the combined wave of Ch-3 and Ch-7 showed a larger value than the others. We can estimate the location of the internal void if we install numerous observation sensors. However, if we use this method to check the integrity of seismic bearings, only two observation sensors are needed.

4. Conclusions

This study analyzed the propagation of elastic waves to detect internal voids in rubber bearings using a nondestructive method. Using a numerical 3D model of a rubber bearing, an external force was applied to the top of a rectangular parallelepiped. The wave propagation was simulated using the CIP method.

The results showed that the internal void can be detected from the combined waves at the observation points facing each other. If the internal void is located only at the center and the void shape is perfectly symmetrical, this method cannot detect the void. However, situations such as this are rare. Internal voids in seismic rubber bearings are usually located near the edge of the bearing because of the excessive shear deformation.

Experimental verification and on-site verification are needed for practical implementation.

5. References

[1] Hayashi K, Adachi Y, Igarashi A, Dang J (2014): Experimental evaluation of aging deterioration of rubber bearings in highway bridges. *2nd European Conference on Earthquake Engineering and Seismology*, Istanbul, Turkey.

[2] Kawasaki Y, Teramura N, Izuno K (2017): Acoustic emission technique for evaluation of damage to laminated rubber bearing. *Journal of JSCE*, **5** (1), 2-9.

[3] Xiao F, Yabe T, Ito T (1996): Constructing oscillation preventing scheme for advection equation by rational function, *Computer Physics Communications*, **93**, 1-12.

[4] Nakamura T, Yabe T (1999): Cubic Interpolate Propagation Scheme for Solving the Hyper-Dimensional Vlasov-Poisson Equation in Phase Space, *Computer Physics Communications*, **120**, 122-154.

[5] Saito J (2009): An Application of the CIP Method to Elastodynamics, *Journal of Applied Mechanics: JSCE*, **12**, 135-137. (in Japanese)

[6] Nose Y, Izuno K, Kawasaki Y (2019): Numerical simulation for detecting internal void of seismic rubber bearing, *Journal of Japan Association for Earthquake Engineering*, **19** (5), 5_283-5_293. (in Japanese)

